The Asynchronous & Irregular State of Cortical Circuits

Candidate 5586A

Part IIB: 4G3 Computational Neuroscience

Abstract

In this report we investigate the asynchronous and irregular dynamical regime of cortical circuits through a simple model network. The model consists of two interconnected populations of "leaky integrate-and-fire" (LIF) neurons which receive inputs from a third external population of "Poisson" neurons whose firing is modelled as a constant rate Poisson process. The interconnected populations consist of a collection of excitatory (E) and inhibitory (I) neurons which communicate with each other through weighted channels and receive their baseline input from the independent external (X) population of neurons. We build the simulation progressively, analysing the strengths and limitations of the model as we go along. We focus on comparing the simulated performance of the network to theoretical predictions and conclude with a discussion of the relatability of the model to neuronal activity in the brain.

Introduction

Neuroscience is a highly inter-disciplinary field engaging people and employing approaches from all areas of science, ranging from molecular and cellular biology to psychology and human psychophysics. Theoretical neuroscience helps to succinctly describe and condense the findings from experimental neuroscience research through the construction of compact representations and the identification of unifying concepts and principles. Computational neuroscience then implements these principles and representations and continues to investigate the information content of neural signals by modelling the nervous system at several structural scales, including the biophysical, the circuit and the systems levels. The discipline combines knowledge of physics, biology, chemistry and mathematics through scientific computing to build insightful simulations and models of the nervous system. This report will deal with the description of one such model and its usefulness as a tool to simulate and contribute to the understanding of the brain.

We focus on the characterisation of a simplified version of a model for the dynamics of neuronal networks that was first designed by van Vreeswijk and Sompolinsky (1996). This model was conceived to showcase the possibility of observing chaos in a system with balanced excitatory and inhibitory activity. It also has the interesting property of being able to self-regulate the excitatory and inhibitory activity to ensure stability. We assemble the model using a bottom-up approach, where we build the network incrementally by adding features which allow it to behave more like a real cortex.

The final goal is to implement and analyse the full network whose architecture is shown in Figure 1. In its final form, the network comprises three populations with N neurons each: one excitatory (E), one inhibitory (I) and one external population (X) which provides the baseline input to the network. Every neuron in the E and I populations receives input from K randomly-chosen neurons in each of the E, I and X populations. The weights associated with the connections from neurons in population β to neurons in population α are given by $J_{\alpha\beta}/\sqrt{K}$ where $\alpha, \beta \in \{\text{E, I, X}\}$ and $J_{\alpha\beta}$ is a constant defining the weight of the connection.

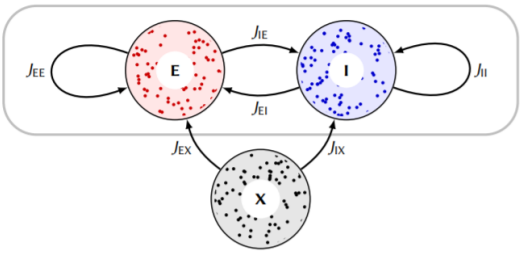

Figure 1: Diagram representing the 3 populations of N neurons and the weights of their respective connections. We note that all connections deriving *from* inhibitory neurons have negative weights $J_{EI}, J_{II} < 0$ whereas connections deriving *from* both the excitatory and external neurons have positive weights $J_{EE}, J_{IE}, J_{EX}, J_{IX} > 0$.

The neurons in X are modelled as independent "Poisson neurons" receiving no inputs from the neurons in E and I. These neurons fire action potentials independently of each other according to a Poisson process with rate r_X. The neurons in E and I are instead modelled as simple "leaky integrate-and-fire" (LIF) neurons. This model of the neuron was pioneered by Louis Lapicque in his seminal article (Lapicque, 1907) and is still one of the most popular models in computational neuroscience for both cellular and neural network studies, owing to its simplicity. The dynamics of an LIF neuron in our model network can be described by a single differential equation, where the membrane potential V_i^α of the i^{th} neuron in population α obeys first-order dynamics given by

$$\frac{dV_i^\alpha(t)}{dt} = -\frac{V_i^\alpha(t)}{\tau} + \sum_{\beta \in \{\text{E, I, X}\}} \frac{J_{\alpha\beta}}{\sqrt{K}} \sum_{j \in C_i^{\alpha\beta}} S_j^\beta(t) \tag{1}$$

where $C_i^{\alpha\beta}$ denotes the set that contains the indices of those K neurons in population β that have been randomly chosen to connect onto the i^{th} neuron of population α, τ is the membrane time constant and $S_j^\beta(t)$ is a Dirac comb function (also known as a 'spike train') marking the timestamps of spikes occurring in the j^{th} neuron of population β.

The last element of the network dynamics is referred to as the 'spike-and-reset' mechanism and consists of modelling action potentials by adding a Dirac delta function to the aforementioned comb function $S_i^\alpha(t)$ whenever $V_i^\alpha(t)$ grows above a threshold value V_{th}. Upon the emission of an action potential, the membrane voltage $V_i^\alpha(t)$ is immediately reset to 0 and the network continues as per Equation 1.

To enable the simulation of this network in software, time had to be discretised and hence all continuous functions i.e. $S(t)$ and $V(t)$ were defined in discrete time by evaluating them at integer multiples of a timestep δ_t. To keep record of when we are dealing with continuous and discrete time processes we adopt the notation

$$\begin{aligned} \widetilde{S}(k) &= S(k\delta_t) \\ \widetilde{V}(k) &= V(k\delta_t) \end{aligned} \tag{2}$$

to denote the discretised spike trains and membrane voltage, respectively, evaluated at the k^{th} timestep.

All throughout our implementation, unless specifically indicated otherwise, we adopted the values presented in Table 1 for the parameters mentioned in the above description of the model

Table 1: Parameter notations, values and descriptions.

Notation	Value	Description
V_{th}	1	spiking threshold
δ_t	0.1ms	integration timestep
τ	20ms	membrane time constant
N	1000	number of neurons in each population
K	100	number of presynaptic partners (per neuron) from each population
r_X	10Hz	firing rate of the Poisson neurons in population X

1 Generating Poisson Spike Trains

We began the implementation procedure by simulating the Poisson process that governs the dynamics of the neurons in population X. For a Poisson process with constant rate r_X the probability of an event occurring between time t and time $t + \delta_t$ (for δ_t very small) is approximately $r_X \delta_t$, independent of t. Thus the discretised Poisson process was simulated by independently sampling the value of $\widetilde{S}(k)$ at each timestep from a Bernoulli distribution which emits a spike of magnitude $1/\delta_t$ with probability $r_X \delta_t$

$$\widetilde{S}(k) \leftarrow \frac{1}{\delta_t} \begin{cases} 1 & \text{with probability } r_X \delta_t \\ 0 & \text{with probability } (1 - r_X \delta_t) \end{cases} \tag{3}$$

where $r_X = 10$Hz is the expected number of spikes fired every second by a neuron in population X and $\delta_t = 0.1$ms is the integration time-step. The simulation was run for 2 seconds (i.e. 20000 iterations using $\delta_t = 0.1$ms) where samples were taken from the above Bernoulli distribution after every iteration for each of the $N = 1000$ neurons in X. The resulting activity was plotted in the form of raster plots as shown in Figure 2.

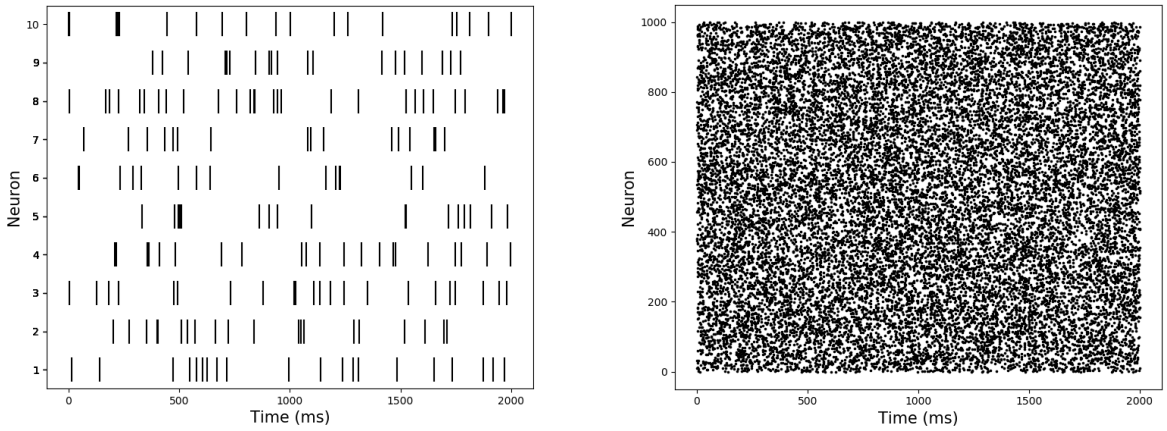

(a) Raster plot over 2 seconds for 10 neurons.

(b) Raster plot over 2 seconds for $N = 1000$ neurons.

Figure 2: Raster plots over 2 seconds for (a) 10 and (b) 1000 Poisson neurons firing at a constant rate of $r_X = 10$Hz. From the plots, we can observe an average of approximately 20 spikes over the course of the 2 seconds, as expected. Figure (a) also shows a phenomenon known to neuroscientists as 'bursts', which occur when a neuron fires repeatedly in a short time interval and then displays a quiescent period much longer than a typical inter-spike interval. These can be identified as dark regions of the raster plot where spikes seem to overlap. From (b) we observe that the raster plot does not show any population-level pattern, as expected from the independent nature of the Poisson neurons in X.

To verify that the simulation had been implemented correctly, we counted the total number of spikes fired by each neuron over the course of the 2 seconds and averaged this number across the $N = 1000$ neurons. According to the Law of Large Numbers (LLN), this empirical value $\mathbb{E}\left[\hat{n}_{spikes}\right]$ should asymptotically approach the value predicted by theory of $\mathbb{E}\left[n_{spikes}\right] = 2\text{s} \cdot r_X = 20$ as N grows large. Reassuringly, for 1000 neurons the average was found to be $\mathbb{E}\left[\hat{n}_{spikes}\right] = 19.9845$. The results for different values of N are shown in Table 2 and can be seen to converge towards 20 for increasing values of N.

Table 2: Empirical average of the number of spikes over 2s for different values of N.

$\mathbf{N}$	$\mathbb{E}\left[\hat{\mathbf{n}}_{\mathbf{spikes}}\right]$
1000	19.9845
10000	20.0046
50000	20.0008

2 Single LIF Neuron with One Input Spike Train

The next step in our implementation considered simulating the voltage dynamics and spiking activity of an LIF neuron receiving input from a single Poisson neuron from population X. The membrane potential dynamics of such a neuron are those of a first order system with time constant τ and the appropriately weighted Poisson spike train as the input

$$\frac{dV_i(t)}{dt} = \frac{-V_i(t)}{\tau} + wS_j(t) \tag{4}$$

where $V_i(t)$ is the membrane potential of the LIF neuron and $S_j(t)$ is the input Poisson spike train. For simulation purposes, the synaptic weight w was set to 0.9. This equation was implemented in discrete time through forward Euler integration as follows

$$\widetilde{V}_i(0) \leftarrow 0 \quad \text{and} \quad \widetilde{V}_i(k) \leftarrow \widetilde{V}_i(k-1) + \delta_t \left[-\frac{\widetilde{V}_i(k-1)}{\tau} + w\widetilde{S}_j(k-1) \right] \tag{5}$$

and the spiking activity was simulated by introducing a threshold V_{th} that triggered the 'spike-and-reset' mechanism whenever it was exceeded by the membrane voltage

$$\widetilde{S}_i(k) \leftarrow \frac{1}{\delta_t} \begin{cases} 1 & \text{if } \widetilde{V}_i(k) > V_{\text{th}} \\ 0 & \text{otherwise} \end{cases} \quad \text{and if } \widetilde{V}_i(k) > V_{\text{th}} \text{ then } \widetilde{V}_i(k) \leftarrow 0 \tag{6}$$

indicating the presence of a spike in the discrete output spike train $\widetilde{S}_i(k)$ and resetting the membrane voltage $\widetilde{V}_i(k)$ to 0. The results of the simulation for a 2-second run are presented in Figure 3

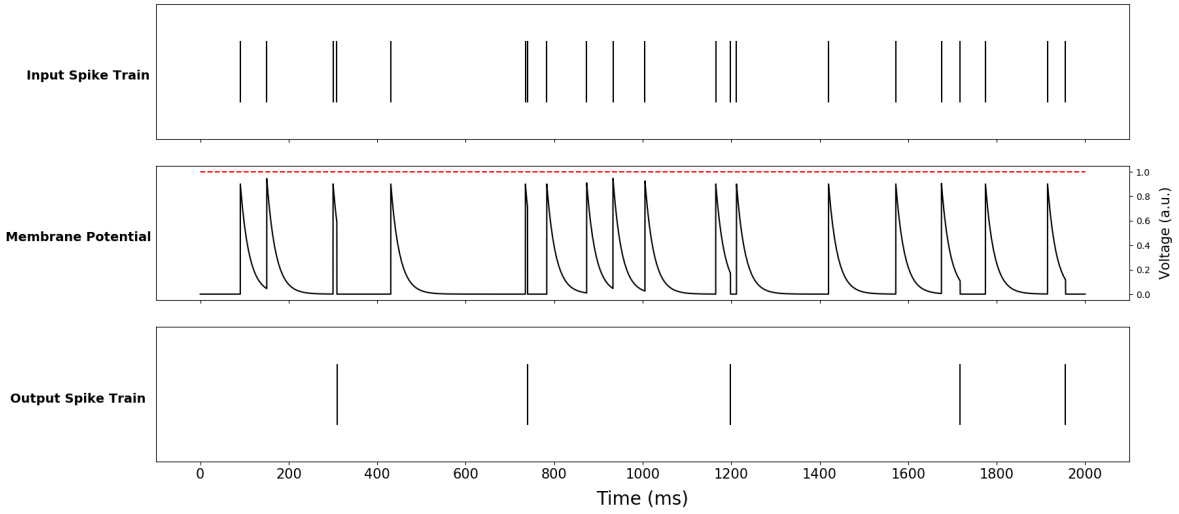

Figure 3: Figure showing the input spike train (top), membrane potential (middle) and output spike train (bottom) for the LIF neuron simulated using eqs. (5) and (6). The threshold membrane potential $V_{th} = 1$ is shown in red. We notice that the peaks in the membrane potential correspond to the timestamps of the input spikes, after which the potential relaxes back to its equilibrium value of 0 with time constant $\tau = 20$ms. We also note that the timestamps of the output spikes correspond to when we observe rapid firing in the input spike train (i.e. short 'bursts').

The simulation showed us that the neuron behaved as expected, peaking at the location of input spikes and then decaying back to its rest potential of 0 with time constant τ. Output spikes were observed when there had been repeated firing in the input spike train, also known as a 'burst'. Bursts cause the LIF neuron's membrane voltage to increase rapidly before it has time to decay, causing it to exceed the threshold and hence create a spike at the output. Notice how we never see the voltage exceed the threshold in Figure 3 as it is instantaneously reset to 0 when an output spike is recorded.

3 Single LIF Neuron with Many Input Spike Trains

3.1 Part A

In this section we further expand on the model of the LIF neuron by considering a single LIF neuron receiving inputs from K independent Poisson neurons, each firing at a constant rate r_X. The K corresponding synaptic weights are all set to a constant w. The dynamics are hence described by

$$\frac{dV_i(t)}{dt} = -\frac{V_i(t)}{\tau} + \underbrace{\frac{w}{K}\sum_{j=1}^{K} S_j(t)}_{h(t)} \tag{7}$$

where $h(t)$ denotes the input to the first order system and the other symbols maintain the same meaning as in Section 2. To simulate these dynamics, the spike-and-reset mechanism was disabled (i.e. $V_i(t)$ was not reset to 0 if it exceeded the threshold V_{th}) and Equation 7 was implemented in discrete-time as described by Equation 8 in Section 3.2.1. For $w = 1$, a 2-second long sample is presented in Figure 4

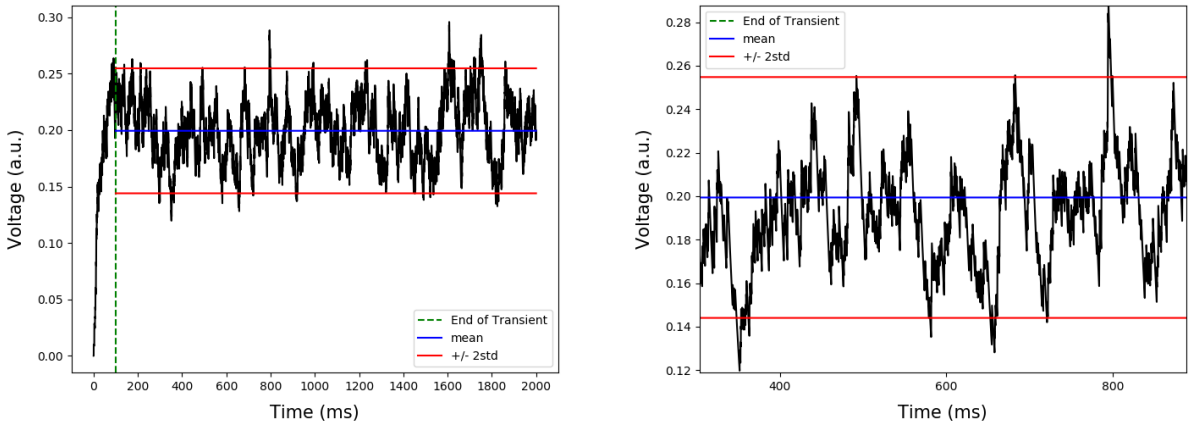

(a) Membrane voltage of LIF neuron over a 2s interval.

(b) Membrane voltage of LIF neuron over a 400ms interval.

Figure 4: Plots showing (a) the full 2-second long sample (b) a 400ms snippet of the dynamics of a single LIF neuron receiving inputs from $K = 100$ independent Poisson neurons firing at a constant rate $r_X = 10$Hz with constant synaptic weights $w = 1$. From (a) we notice how the oscillations become stationary and approximately normally distributed with constant mean (blue) and standard deviation (red) after the initial transient of approximately 100ms (green). (b) is a zoomed-in version of (a) showing the scale of the oscillations. We notice how the spiking activity of the input neurons introduces jagged edges and rapid changes in the voltage, which are typical of real electrophysiological recordings.

3.2 Part B

The fluctuations of $V_i(t)$ in Section 3.1 were observed to become stationary after approximately 100ms, with a distribution which can be considered Gaussian with mean μ and variance σ^2. By first calculating the mean and covariance function of $h(t)$, below we derive the theoretical values of μ and σ^2 as functions of w, K, r_X and τ.

3.2.1 Derivation of Mean and Covariance Function of $h(t)$

We begin by writing Equation 7 in discrete time

$$\widetilde{V}(k) \leftarrow \widetilde{V}(k-1) + \delta_t \Bigg[-\frac{\widetilde{V}(k-1)}{\tau} + \underbrace{\frac{w}{K}\sum_{j=1}^{K} \widetilde{S}_j(k-1)}_{\widetilde{h}(k)} \Bigg] \tag{8}$$

which facilitates the derivation of the expression for the mean and variance of the fluctuations of $V_i(t)$. Notice that we have dropped the subscript i for convenience and without scope for confusion. However, before starting with the derivation for $\widetilde{V}(k)$, we start by finding the mean and covariance function for $\widetilde{h}(k)$ as it will prove useful later

$$\begin{aligned}\mathbb{E}\left[\widetilde{h}(k)\right] = \mathbb{E}\left[\frac{w}{K}\sum_{j=1}^{k}\widetilde{S}_j(k-1)\right] &= \frac{w}{K}\,\mathbb{E}\left[\sum_{j=1}^{k}\widetilde{S}_j(k-1)\right] \\ &= \frac{w}{K}\sum_{j=1}^{k}\mathbb{E}\left[\widetilde{S}_j(k-1)\right] \\ &= \frac{w}{K}\sum_{j=1}^{K} r_X\delta_t \cdot \frac{1}{\delta_t} \\ &= wr_X \end{aligned} \tag{9}$$

where we have used the fact that, for a Poisson process with constant rate r_X, the probability of a spike falling between t and $t+\delta_t$ (for very small δ_t) is approximately $r_X\delta_t$, independent of t. Thus, a discretised Poisson process can be generated by sampling the value $\widetilde{S}_j(k-1)$ in each bin independently from a Bernoulli distribution

$$\widetilde{S}_j(k-1) \leftarrow \frac{1}{\delta_t}\begin{cases}1 & \text{with probability } r_X\delta_t \\ 0 & \text{with probability } 1-r_X\delta_t\end{cases} \tag{10}$$

The result in Equation 9 makes intuitive sense, since we expect the activity from K independent Poisson neurons firing at a constant rate r_X to have an average rate of Kr_X and hence if we define the amplitude of the spike to be $1/\delta_t$ we expect an average amplitude at a specific time instant to be $Kr_X\delta_t/\delta_t = Kr_X$. If we now multiply this by the normalised synaptic weight w/K, we obtain an average input at any specific time instant of wr_X.

The covariance function of $\widetilde{h}(k)$ can be calculated similarly

$$\begin{aligned}\mathbf{cov}\left(\widetilde{h}(k),\,\widetilde{h}(k')\right) &= \mathbb{E}\left[\left(\widetilde{h}(k)-\mathbb{E}\left[\widetilde{h}(k)\right]\right)\left(\widetilde{h}(k')-\mathbb{E}\left[\widetilde{h}(k')\right]\right)\right] \\ &= \mathbb{E}\left[\left(\widetilde{h}(k)-wr_X\right)\left(\widetilde{h}(k')-wr_X\right)\right] \\ &= \mathbb{E}\left[\widetilde{h}(k)\widetilde{h}(k')\right] - w^2r_X^2 \end{aligned} \tag{11}$$

where we have used the result from Equation 9 to go from the first to the second and from the second to the third line. We now derive the expression for $\mathbb{E}\left[\widetilde{h}(k)\widetilde{h}(k')\right]$ as follows

$$\begin{aligned}\mathbb{E}\left[\widetilde{h}(k)\widetilde{h}(k')\right] &= \mathbb{E}\left[\frac{w}{K}\sum_{i=1}^{K}\widetilde{S}_i(k-1)\frac{w}{K}\sum_{j=1}^{K}\widetilde{S}_j(k'-1)\right] \\ &= \frac{w^2}{K^2}\,\mathbb{E}\left[\sum_{i=1}^{K}\sum_{j=1}^{K}\widetilde{S}_i(k-1)\widetilde{S}_j(k'-1)\right] \\ &= \frac{w^2}{K^2}\sum_{i=1}^{K}\sum_{j=1}^{K}\mathbb{E}\left[\widetilde{S}_i(k-1)\widetilde{S}_j(k'-1)\right] \end{aligned} \tag{12}$$

where from Equation 10 we find

$$\mathbb{E}\left[\widetilde{S}_i(k-1)\widetilde{S}_j(k'-1)\right] = \begin{cases} (1/\delta_t)^2 \cdot (r_X\delta_t)^2 = r_X^2 & i = j \text{ and } k \neq k' \\ (1/\delta_t)^2 \cdot (r_X\delta_t) = r_X/\delta_t & i = j \text{ and } k = k' \\ r_X^2 & i \neq j \text{ and } k \neq k' \\ r_X^2 & i \neq j \text{ and } k = k' \end{cases} \tag{13}$$

hence, plugging this into the expression in Equation 12 gives

$$\mathbb{E}\left[\widetilde{h}(k)\widetilde{h}(k')\right] = \begin{cases} w^2 r_X^2 & k \neq k' \\ \frac{w^2 r_X}{K}\left(\frac{1}{\delta_t} + r_X(K-1)\right) & k = k' \end{cases} \tag{14}$$

And finally the covariance function of $h(t)$ in discrete time is

$$\mathbf{cov}\left(\widetilde{h}(k), \widetilde{h}(k')\right) = \begin{cases} 0 & k \neq k' \\ \frac{w^2 r_X}{K}\left(\frac{1}{\delta_t} - r_X\right) & k = k' \end{cases} \tag{15}$$

This implies that the input spike trains do not depend on their past or future values and are hence completely time-independent, as expected from a sum of independent Poisson neurons.

3.2.2 Derivation of Mean and Variance of $V_i(t)$

Returning to the expression for the dynamics of an LIF neuron receiving inputs from K Poisson neurons in discrete form

$$\widetilde{V}(k) \leftarrow \widetilde{V}(k-1) + \delta_t\left[-\frac{\widetilde{V}(k-1)}{\tau} + \widetilde{h}(k)\right] \tag{16}$$

using the results from Section 3.2.1 we can now find the mean and variance of $V_i(t)$ after transient activity has decayed. We start by deriving the expression for the mean of the stationary distribution of $V_i(t)$

$$\begin{aligned} \mathbb{E}\left[\widetilde{V}(k)\right] &= \mathbb{E}\left[\widetilde{V}(k-1) + \delta_t\left(-\frac{\widetilde{V}(k-1)}{\tau} + \widetilde{h}(k)\right)\right] \\ &= \mathbb{E}\left[\widetilde{V}(k)\right] - \frac{\delta_t}{\tau}\,\mathbb{E}\left[\widetilde{V}(k)\right] + \delta_t\,\mathbb{E}\left[\widetilde{h}(k)\right] \end{aligned} \tag{17}$$

where we have gone from the first to the second line using the property of stationary distributions to state that $\mathbb{E}\left[\widetilde{V}(k)\right] = \mathbb{E}\left[\widetilde{V}(k-1)\right]$. Now replacing the expression for $\mathbb{E}\left[\widetilde{h}(k)\right]$ from Equation 9 and re-arranging gives

$$\begin{aligned} \mathbb{E}\left[\widetilde{V}(k)\right] &= (1 - \frac{\delta_t}{\tau})\,\mathbb{E}\left[\widetilde{V}(k)\right] + \delta_t w r_X \\ \therefore \mu = \mathbb{E}\left[\widetilde{V}(k)\right] &= \tau w r_X \end{aligned} \tag{18}$$

We now derive the expression for the variance of $V_i(t)$. We begin with the definition of the variance of a random variable

$$\begin{aligned} \mathbf{Var}\left[\widetilde{V}(k)\right] &= \mathbb{E}\left[\widetilde{V}(k)^2\right] - \left(\mathbb{E}\left[\widetilde{V}(k)\right]\right)^2 \\ &= \mathbb{E}\left[\widetilde{V}(k)^2\right] - (\tau w r_X)^2 \end{aligned} \tag{19}$$

To derive the expression for $\mathbb{E}\left[\widetilde{V}(k)^2\right]$ we expand $\widetilde{V}(k)$ using Equation 16 to get

$$\begin{aligned}
\mathbb{E}\left[\widetilde{V}(k)^2\right] &= \mathbb{E}\left[\left(\widetilde{V}(k-1) - \frac{\delta_t \widetilde{V}(k-1)}{\tau} + \delta_t \widetilde{h}(k)\right)^2\right] \\
&= \mathbb{E}\left[\left(\widetilde{V}(k-1)\left(1 - \frac{\delta_t}{\tau}\right) + \delta_t \widetilde{h}(k)\right)^2\right] \\
&= \left(1 - \frac{\delta_t}{\tau}\right)^2 \mathbb{E}\left[\widetilde{V}(k-1)^2\right] + \delta_t^2 \,\mathbb{E}\left[\widetilde{h}(k)^2\right] + 2\delta_t \left(1 - \frac{\delta_t}{\tau}\right) \mathbb{E}\left[\widetilde{h}(k)\widetilde{V}(k-1)\right] \\
&= \left(1 - \frac{\delta_t}{\tau}\right)^2 \mathbb{E}\left[\widetilde{V}(k)^2\right] + \delta_t^2 \frac{w^2 r_X}{K}\left(\frac{1}{\delta_t} + r_X(K-1)\right) + 2\delta_t \left(1 - \frac{\delta_t}{\tau}\right) \mathbb{E}\left[\widetilde{h}(k)\widetilde{V}(k-1)\right] \qquad (20)
\end{aligned}$$

where the last step uses the properties of stationarity to state that $\mathbb{E}\left[\widetilde{V}(k-1)^2\right] = \mathbb{E}\left[\widetilde{V}(k)^2\right]$ and replaces the expression for $\mathbb{E}\left[\widetilde{h}(k)^2\right]$ from Equation 14. We now note that $\mathbb{E}\left[\widetilde{h}(k)\widetilde{V}(k-1)\right]$ = $\mathbb{E}\left[\widetilde{h}(k)\right]\mathbb{E}\left[\widetilde{V}(k-1)\right]$ since $\widetilde{V}(k-1)$ only depends on $\widetilde{h}(k-1)$ and is hence independent from $\widetilde{h}(k)$, as shown in Equation 15. This gives

$$\begin{aligned}
\mathbb{E}\left[\widetilde{h}(k)\widetilde{V}(k-1)\right] = \mathbb{E}\left[\widetilde{h}(k)\right]\mathbb{E}\left[\widetilde{V}(k-1)\right] = \mathbb{E}\left[\widetilde{h}(k)\right]\mathbb{E}\left[\widetilde{V}(k)\right] \\
\therefore \mathbb{E}\left[\widetilde{h}(k)\widetilde{V}(k-1)\right] = \tau w^2 r_X^2 \qquad (21)
\end{aligned}$$

hence plugging this result into Equation 20 gives

$$\begin{aligned}
\mathbb{E}\left[\widetilde{V}(k)^2\right] = \left(1 - \frac{\delta_t}{\tau}\right)^2 \mathbb{E}\left[\widetilde{V}(k)^2\right] + \frac{w^2 r_X}{K}\left(\delta_t + r_X \delta_t^2 (K-1)\right) + 2\delta_t \left(1 - \frac{\delta_t}{\tau}\right)\tau w^2 r_X^2 \\
\therefore \mathbb{E}\left[\widetilde{V}(k)^2\right] = \frac{\tau^2 w^2 r_X \left(1 - r_X \delta_t (K+1) + 2K\tau r_X\right)}{K\left(2\tau - \delta_t\right)} \qquad (22)
\end{aligned}$$

and plugging this into Equation 19 gives us the expression for the variance

$$\begin{aligned}
\sigma^2 = \mathbf{Var}\left[\widetilde{V}(k)\right] &= \mathbb{E}\left[\widetilde{V}(k)^2\right] - \left(\mathbb{E}\left[\widetilde{V}(k)\right]\right)^2 \\
&= \frac{\tau^2 w^2 r_X \left(1 - r_X \delta_t (K+1) + 2K\tau r_X\right)}{K\left(2\tau - \delta_t\right)} - (\tau w r_X)^2 \\
&= \frac{w^2 r_X \tau^2 (1 - \delta_t r_X)}{\left(2\tau - \delta_t\right) K} \qquad (23)
\end{aligned}$$

If we let $\delta_t \to 0$, or simply note that it is small compared to the other terms in the expression, we obtain an approximation of the variance in terms of w, K, r_X and τ

$$\sigma^2 \approx \frac{w^2 r_X \tau^2}{2\tau K} = \frac{w^2 r_X \tau}{2K} \qquad (24)$$

3.3 Part C

To confirm the correctness of our implementation of the single LIF neuron receiving inputs from K independent Poisson neurons, we plotted the theoretical expressions for μ and σ^2 from Section 3.2.2 as a function of K (keeping the other parameters fixed at their default values in Table 1 and $w = 1$) and superimposed the values obtained from simulations for $K = 1, 10, 100$ and 1000. The resulting plots are shown in Figure 5

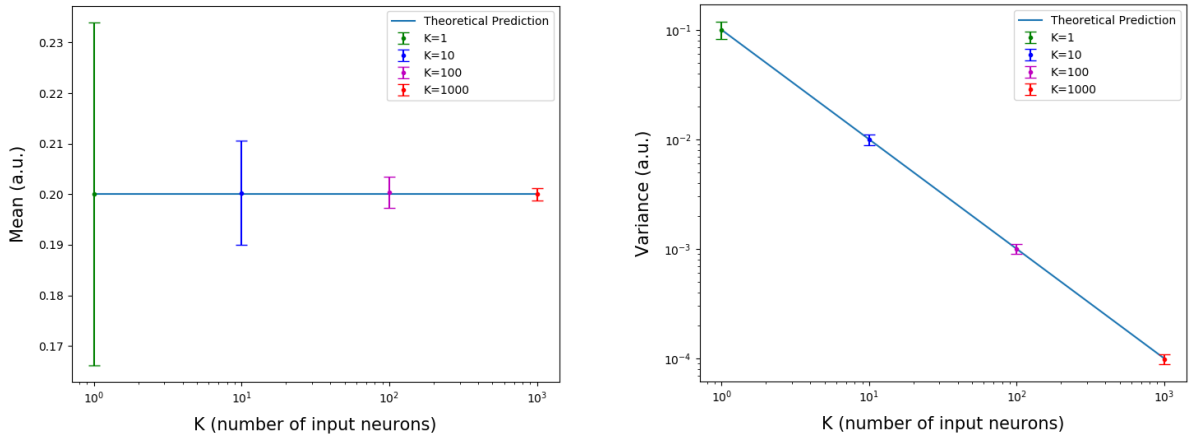

(a) Theoretical and empirical values of μ for different K.

(b) Theoretical and empirical values of σ^2 for different K.

Figure 5: Plots of theoretical and empirical values of μ and σ^2 as a function of K. Both plots show the smooth curves representing the dependence (independence) of the theoretical predictions of μ and σ^2 on K and superimpose the values computed from the simulations for $K = 1, 10, 100, 1000$ with $w = 1$. The empirical values were taken as the average over 50 simulations for each value of K. Each simulation was run for 15s to have enough data to accurately measure the mean and variance of the stationary distribution, and the initial 100ms transient was removed. We note how the theoretical predictions agree well with the empirical observations, confirming the correct implementation of the LIF neuron and, vice versa, the correctness of the derived expressions. It is interesting to notice how the empirical observations of μ (and, to a lesser extent, σ^2) become less noisy as K increases.

The results of the comparison showed a good correspondence between the theoretical and empirical values of μ and σ^2, although an interesting phenomenon was observed whereby the variance of the observations for μ decreased with increasing K. This can be explained by looking at the expression for the theoretical value of σ^2 in Equation 24, which is inversely proportional to K. This indicates that, at lower values of K, the higher variance of the stationary distribution will naturally give rise to more noisy estimates of the mean. In fact, when the estimates were computed using longer simulation times, the variance of the estimates decreased for all values of K (with the decrease being more significant for lower values of K).

Another reason for the discrepancy between the empirical and theoretical values, especially for $K = 1$, is that the membrane potential does not have a perfectly normally distributed stationary distribution. It is important to notice that the gaussianity assumption of the stationary distribution is only accurate for large values of K, due to the central limit theorem (CLT). This further explains why the estimates become better for larger values of K. This point is elaborated upon through Figures 6 and 7.

To more easily compare the theoretical and simulation values for μ and σ^2 we present two more figures, Figure 6 and Figure 7. The first superimposes the empirical and theoretical values of μ and σ^2 as horizontal mean and $\pm 2\sigma$ lines on plots of the membrane potential for the different values of K

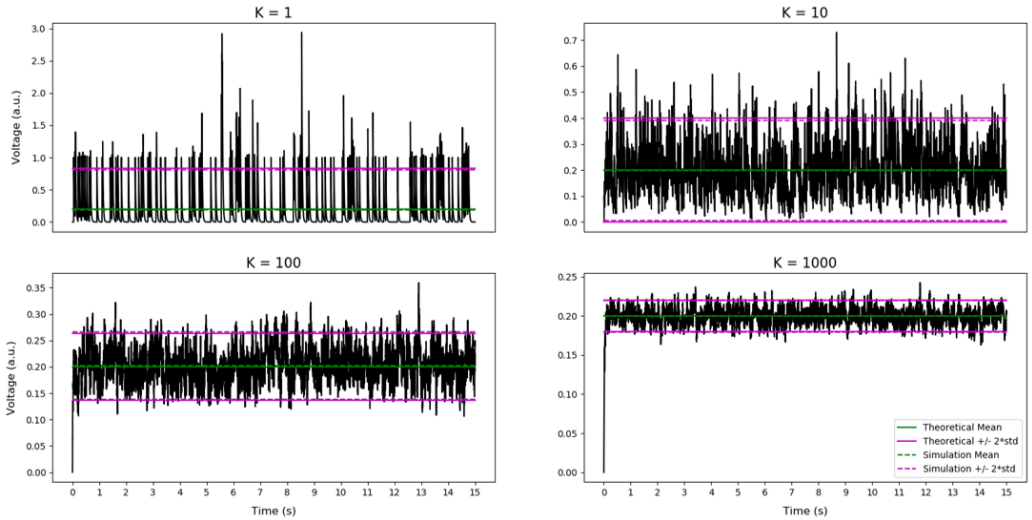

Figure 6: Plots of 15-second simulations of the membrane potential for $K = [1, 10, 100, 1000]$ with the empirical (dashed) and theoretical (solid) mean (green) and standard deviations (magenta) superimposed. Notice how the theoretical and empirical estimates agree fairly well. We, however, observe that the membrane potential for $K = 1$ does not display a normally distributed stationary distribution, and for $K = 10$ the distribution is slightly right-skewed.

Figure 6 reveals that the membrane potential for $K = 1$ does not actually present a normally distributed stationary distribution. This is because the LIF neuron does not receive enough excitatory input from its single input Poisson neuron to present sustained fluctuations around a non-zero mean. We instead observe a peaky voltage plot which peaks whenever the single input neuron fires, and relaxes back to 0 in the subsequent timesteps. This means that the theoretical expressions for μ and σ^2 do not accurately model the behaviour for $K = 1$, hence explaining why it was the case presenting the worst correspondence with empirical values in Figure 5.

Figure 7 emphasizes this finding by overlaying the probability density functions defined by the theoretical values of μ and σ^2 on a histogram of the empirical observations of the membrane potential. We observe a good fit for $K = 100$ and 1000, but the data for $K = 1$ is clearly not normally distributed, although its mean and variance do not deviate significantly from those predicted by the theoretical expressions due to the stationarity of the input Poisson neuron. For $K = 10$ we can more clearly observe the aforementioned right-skewedness of the empirical distribution.

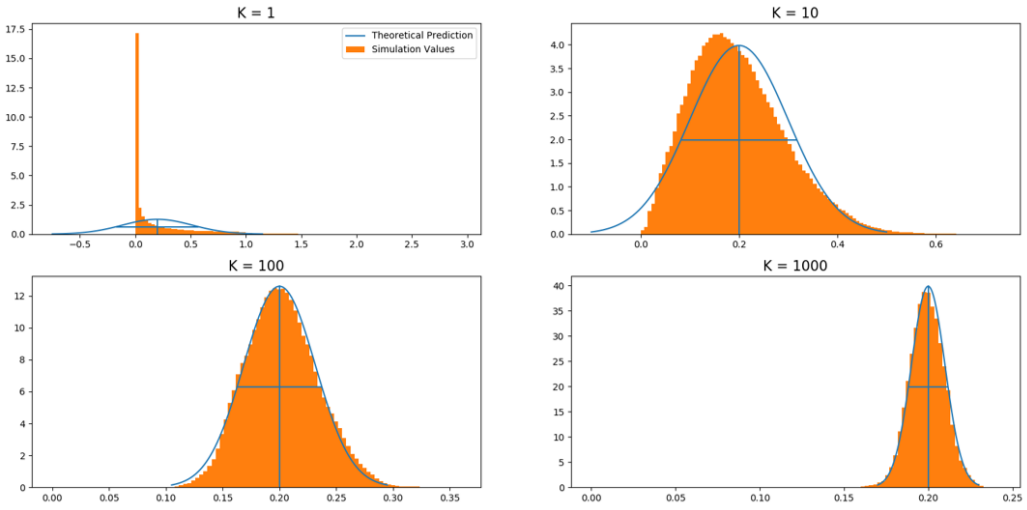

Figure 7: Probability density functions defined by the theoretical expressions for μ and σ^2 (blue) overlaid on the empirical distributions (i.e. normalised histograms with $n_{bins} = 100$, in orange) of the membrane potential for $K = [1, 10, 100, 1000]$. Notice the non-gaussianity of the distribution for $K = 1$, the skewedness of the distribution for $K = 10$ and the better agreement of the theoretical parameters with simulation values for increasing K (as per the CLT).

3.4 Part D

We now use the expression for μ from Section 3.2.2 to calculate the value that w must take such that, whatever the value of K, the mean potential is equal to V_{th}

$$\begin{aligned} \mu &= \tau w r_X = V_{th} \\ \therefore w &= \frac{V_{th}}{\tau r_X} \end{aligned} \tag{25}$$

and with $V_{th} = 1$, $\tau = 20$ms and $r_X = 10$Hz we get

$$w = \frac{1}{0.02\text{s} \cdot 10\text{Hz}} = 5 \tag{26}$$

With this value of w and the 'reset' component of the 'spike-and-reset' mechanism disabled, theory would predict that the neuron be firing for half the duration of the simulation. It was evident from the expression for the dynamics of the membrane potential in Equation 7 that the synaptic weight would have to be increased from $w = 1$ to increase the mean potential. This is because we are only modelling excitatory neurons in this intermediate model of the LIF neuron. In Section 4 we will incorporate inhibitory Poisson neurons to our simulations.

The theoretically predicted value for w in Equation 26 was tested in our simulation of a single LIF neuron receiving inputs from $K = 100$ Poisson neurons by setting $w = 5$. The resulting dynamics of the membrane potential over 2 seconds are shown in Figure 8

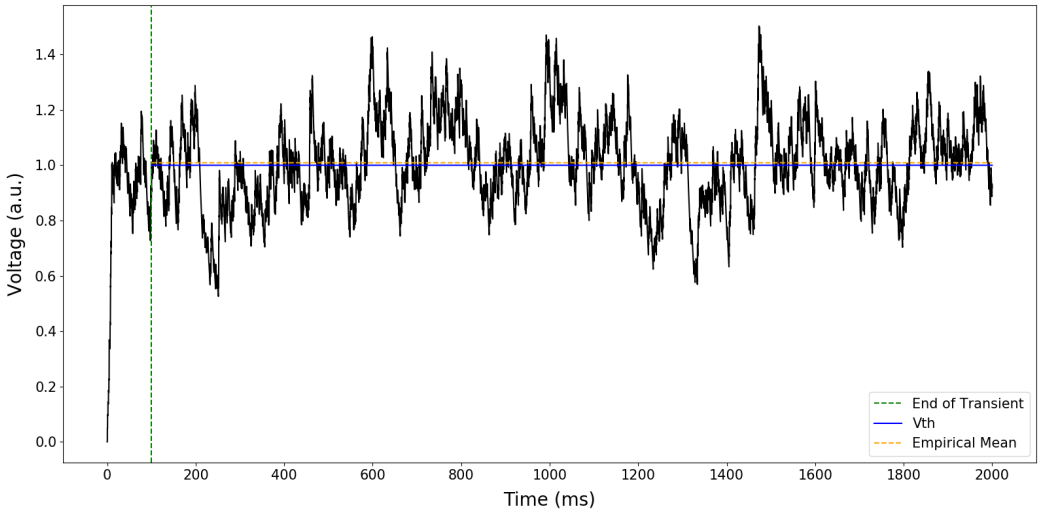

Figure 8: Plot of the membrane potential for the 2-second long simulation of an LIF neuron receiving input from $K = 100$ Poisson neurons with synaptic weight $w = 5$. We observe that the theoretical prediction of the value of w required to make $\mu = V_{th} = 1$ has indeed allowed us to bring the mean of the membrane voltage oscillations very close to the threshold at a value of 1.009. This once again confirms the correctness of our analytical expression for the mean of the stationary distribution.

3.5 Part E

In our last investigation of the model for a single LIF neuron receiving inputs from K independent Poisson neurons, the spike-and-reset mechanism was re-enabled and we proceeded by trial and error to find the value of w that makes the output firing rate approximately equal to 10Hz (with all other parameters remaining constant). The value found was $w = 4.275$, giving an output firing rate of $r_{output} = 10.15$Hz when averaged over 100 seconds. The first 5 seconds of the resulting activity are shown in Figure 9 below

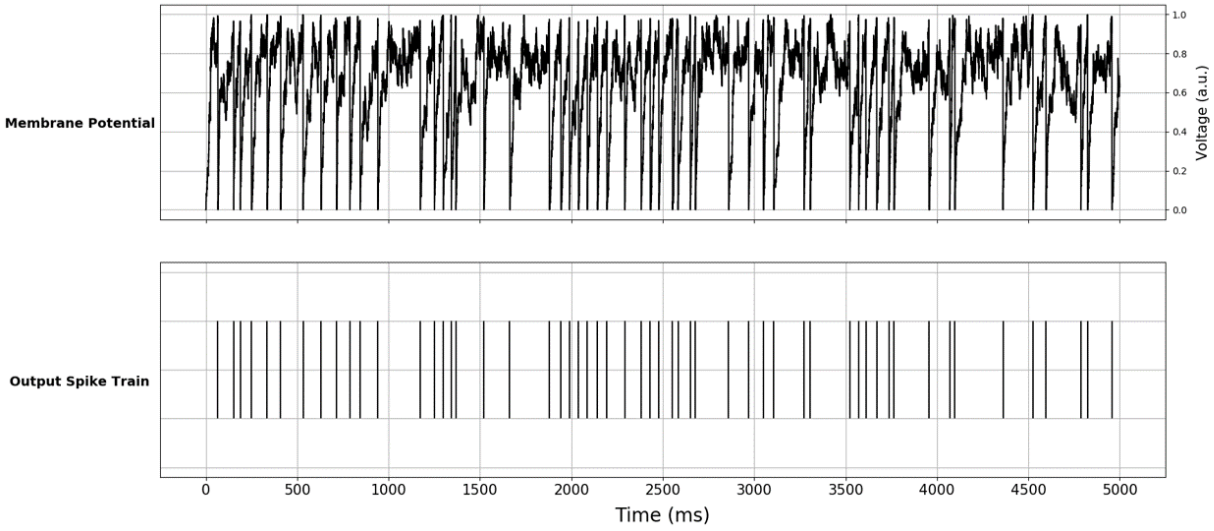

Figure 9: Plot of the membrane potential (top) and the output spike train (bottom) of an LIF neuron receiving input from $K = 100$ Poisson neurons with $w = 4.275$ and the spike-and-reset mechanism activated. The behaviour of the neuron was simulated over 100 seconds of which the plot shows the first 5 seconds. The output firing rate for this choice of w was approximately $r_{output} = 10.15$Hz. Note how the membrane potential spends most of its time in the 100ms-long transient, after which it crosses the threshold $V_{th} = 1$ and is reset to 0, returning to the transient activity. This causes the output firing pattern to be fairly regular over time.

For this value of w, the Fano factor of the output spike train was computed using a counting window of 100ms. The Fano factor is defined as the variance of the number of spikes in each T-second counting window σ_T^2 divided by the mean of the spike count in each window r_T

$$F(T) = \frac{\sigma_T^2}{r_T} \tag{27}$$

and was found to be approximately $F(T) = 0.4831$ for $T = 100$ms. Since our firing rate was fixed to $r_{output} = 10.15$Hz by our choice of w, this gave a mean spike count of approximately $r_T = 1$ in each window and the Fano factor was hence completely determined by the variance of the spiking, which was around $\sigma_T^2 = 0.49$. This Fano factor represents a much lower spike count variability than that usually measured in the cortex, which typically yields Fano factors of more than 1. This hence shows that the model is not accurately representing real spiking dynamics. This lower variability has two main causes:

1. The fact that we have not included inhibitory inputs in our model of the LIF neuron. These bring the mean of the membrane potential μ down to the reset voltage (i.e. 0) and hence avoid the 100ms transient which regularises spiking activity.
2. The fact that we have assumed independent (and time-independent) inputs to the LIF neuron with our input Poisson neurons, something which is not true of a neuron in a real cortex. The inclusion of dependent inputs increases the variability of the spiking input and consequently of the spiking output.

The first point will be addressed in Section 4 which will show how the Fano factor is increased to more realistic levels upon the inclusion of an inhibitory population of neurons. Both the first and second points will be addressed in the simulation of the full network, as described in the introduction, implemented in Section 5.

4 Single LIF Neuron with Many E and I Poisson Inputs

We now consider the case of a single LIF neuron receiving both excitatory and inhibitory input from two different collections of K independent Poisson neurons firing at a constant rate r_X. We take the corresponding K excitatory (resp. inhibitory) synaptic weights to be $w/\sqrt{K}$ (resp. $-w/\sqrt{K}$). The expression describing the discrete dynamics of the membrane potential of this LIF neuron is hence

$$\begin{aligned}\widetilde{V}(k) &\leftarrow \widetilde{V}(k-1) + \delta_t \left[-\frac{\widetilde{V}(k-1)}{\tau} + \frac{w}{\sqrt{K}} \sum_{j=1}^{K} \widetilde{S}_j^E(k-1) - \frac{w}{\sqrt{K}} \sum_{p=1}^{K} \widetilde{S}_p^I(k-1) \right] \\ &\leftarrow \left(1 - \frac{\delta_t}{\tau}\right) \widetilde{V}(k-1) + \delta_t \sqrt{K} \left(\widetilde{h}^E(k) - \widetilde{h}^I(k) \right) \end{aligned} \tag{28}$$

where E and I represent excitatory and inhibitory contributions respectively and all the other terms maintain the same definition as in Section 3.2.1 (especially $\widetilde{h}(k)$, defined as before with unchanged synaptic weights w/K). This expression will be useful to simulate the dynamics and also to derive the theoretical mean μ and variance σ^2 of the membrane potential for this model.

4.1 Part A

We begin by deriving an expression for the mean μ of the stationary distribution of the membrane potential $V_i(t)$ by taking expectations over k on both sides of Equation 28

$$\begin{aligned}\mathbb{E}\left[\widetilde{V}(k)\right] &= \mathbb{E}\left[\left(1 - \frac{\delta_t}{\tau}\right) \widetilde{V}(k-1) + \delta_t \sqrt{K} \left(\widetilde{h}^E(k) - \widetilde{h}^I(k) \right) \right] \\ &= \left(1 - \frac{\delta_t}{\tau}\right) \mathbb{E}\left[\widetilde{V}(k-1)\right] + \delta_t \sqrt{K}\, \mathbb{E}\left[\widetilde{h}^E(k) - \widetilde{h}^I(k) \right] \\ &= \left(1 - \frac{\delta_t}{\tau}\right) \mathbb{E}\left[\widetilde{V}(k)\right] + \delta_t \sqrt{K} \left(\mathbb{E}\left[\widetilde{h}^E(k)\right] - \mathbb{E}\left[\widetilde{h}^I(k)\right] \right) \end{aligned} \tag{29}$$

where we have used the property of stationarity to say that $\mathbb{E}\left[\widetilde{V}(k-1)\right] = \mathbb{E}\left[\widetilde{V}(k)\right]$. We now note that $\mathbb{E}\left[\widetilde{h}^E(k-1)\right] = \mathbb{E}\left[\widetilde{h}^I(k-1)\right] = wr_X$ from Equation 9 in Section 3.2.1 and use this in the equation above

$$\begin{aligned}\frac{\delta_t}{\tau}\, \mathbb{E}\left[\widetilde{V}(k)\right] &= \delta_t \sqrt{K} \left(w r_X - w r_X \right) = 0 \\ \therefore \mu &= \mathbb{E}\left[\widetilde{V}(k)\right] = 0 \end{aligned} \tag{30}$$

Notice the difference between this value of μ and that derived for the case without inhibitory inputs in Section 3.2.2. We now have a zero mean, in contrast to the non-zero mean we had before. This will considerably change the dynamics of the output spike train for the LIF neuron.

We now derive the expression for the variance of the stationary distribution of $V_i(t)$. Using the expression for the discrete dynamics in Equation 28 we write

$$\begin{aligned}\mathbf{Var}\left[\widetilde{V}(k)\right] &= \mathbf{Var}\left[\left(1 - \frac{\delta_t}{\tau}\right) \widetilde{V}(k-1) + \delta_t \sqrt{K} \left(\widetilde{h}^E(k) - \widetilde{h}^I(k) \right) \right] \\ &= \left(1 - \frac{\delta_t}{\tau}\right)^2 \mathbf{Var}\left[\widetilde{V}(k-1)\right] + \delta_t^2 K \mathbf{Var}\left[\widetilde{h}^E(k) - \widetilde{h}^I(k) \right] \end{aligned} \tag{31}$$

where we have used the fact that

$$\mathbf{Var}\left[X + Y\right] = \mathbf{Var}\left[X\right] + \mathbf{Var}\left[Y\right] + 2\mathbf{cov}\left(X, Y\right) \tag{32}$$

where

$$X = \left(1 - \frac{\delta_t}{\tau}\right) \widetilde{V}(k-1) \quad \text{and} \quad Y = \delta_t \sqrt{K} \left(\widetilde{h}^E(k) - \widetilde{h}^I(k)\right) \tag{33}$$

giving

$$\mathbf{Var}\left[X\right] = \left(1 - \frac{\delta_t}{\tau}\right)^2 \mathbf{Var}\left[\widetilde{V}(k-1)\right], \;\; \mathbf{Var}\left[Y\right] = \delta_t^2 K \mathbf{Var}\left[\widetilde{h}^E(k) - \widetilde{h}^I(k)\right], \quad \mathbf{cov}\left(X, Y\right) = 0 \tag{34}$$

where the last equality comes from the independence of the difference between input spike trains $\widetilde{h}^E(k) - \widetilde{h}^I(k)$ and the voltage $\widetilde{V}(k-1)$. This is because the voltage $\widetilde{V}(k-1)$ only depends on the inputs $\widetilde{h}^E(k-1) - \widetilde{h}^I(k-1)$ since the Poisson neurons in E and I fire independently of k and of each other by assumption. Using a similar argument, the variance of the difference between input spike trains can be expanded as

$$\mathbf{Var}\left[\widetilde{h}^E(k) - \widetilde{h}^I(k)\right] = \mathbf{Var}\left[\widetilde{h}^E(k)\right] + \mathbf{Var}\left[\widetilde{h}^I(k)\right] \tag{35}$$

since each spike train is independent and hence two sums of different spike trains will also be independent, giving $\mathbf{cov}\left(\widetilde{h}^E(k), \widetilde{h}^I(k)\right) = 0$. We can now plug the expression for the variance of $\widetilde{h}(k)$ from Equation 15 in Section 3.2.1 into Equation 35 to get

$$\mathbf{Var}\left[\widetilde{h}^E(k) - \widetilde{h}^I(k)\right] = 2\frac{w^2 r_X}{K}\left(\frac{1}{\delta_t} - r_X\right) \tag{36}$$

Using this result and the property of stationarity in Equation 31 yields

$$\mathbf{Var}\left[\widetilde{V}(k)\right] = \left(1 - \frac{\delta_t}{\tau}\right)^2 \mathbf{Var}\left[\widetilde{V}(k)\right] + \delta_t^2 K \left[2\frac{w^2 r_X}{K}\left(\frac{1}{\delta_t} - r_X\right)\right] \tag{37}$$

and rearranging

$$\begin{aligned} \therefore \sigma^2 = \mathbf{Var}\left[\widetilde{V}(k)\right] &= \frac{2\delta_t^2 w^2 r_X \left(\frac{1}{\delta_t} - r_X\right)}{\left(1 - \left(1 - \frac{\delta_t}{\tau}\right)^2\right)} \\ &= \frac{2w^2\tau^2 r_X(1 - r_X\delta_t)}{2\tau - \delta_t} \end{aligned} \tag{38}$$

We can now approximate this expression by taking $\delta_t \to 0$, or by noting that it is small compared to the other terms, in order to express the variance only in terms of w, r_X and τ

$$\begin{aligned} \sigma^2 &= \frac{2w^2\tau^2 r_X(1 - r_X\delta_t)}{2\tau - \delta_t} \\ &\approx \frac{2w^2\tau^2 r_X}{2\tau} \\ &\approx w^2 \tau r_X \end{aligned} \tag{39}$$

Notice that the only difference between this expression for the variance and that of Section 3.2.2 is that we no longer have a factor of $1/2K$ multiplying the $w^2 r_X \tau$ term. This implies that the variance of the membrane potential for this model of the LIF neuron will be a factor of $2K$ larger than in that of Section 3. We will also no longer observe decreasing values of the variance as the number of input neurons increases. Both the expressions were compared to values obtained from simulations with the spike-and-reset mechanism disabled and were found to agree fairly well. We now study the effect that this new model has on the Fano factor of the output spike train.

4.2 Part B

As in Section 3.5, the spike-and-reset mechanism was activated and the value of w such that the LIF neuron fires an average of 10 spikes per second was found by trial and error (with all other parameters remaining constant). The value of w found for this model was approximately $w = 1.55$, giving an output firing rate of $r_{output} = 10.7$Hz averaged over 100 seconds. The first 5 seconds of the resulting activity can be seen in Figure 10 below

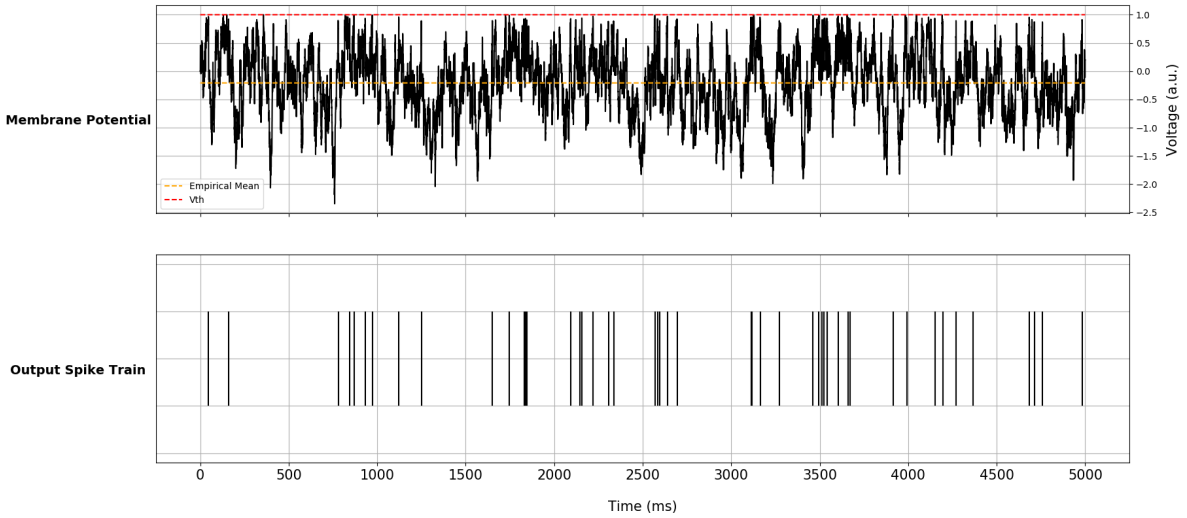

Figure 10: Plot of the membrane potential (top) and output spike train (bottom) of an LIF neuron receiving inputs from K excitatory Poisson neurons and K inhibitory Poisson neurons with $w = 1.55$ and the spike-and-reset mechanism activated. The behaviour of the neuron was simulated over 100 seconds of which the plot shows the first 5 seconds. The output firing rate for this choice of w was approximately $r_{output} = 10.7$Hz. Note how the membrane potential maintains its stationary distribution all throughout the simulation since the spike-and-reset mechanism does not affect this due to the distribution's zero mean (orange). We hence observe a much more variable spike train at the output which can now allow spikes to fire closer to each other than before, giving more scope for bursts (darker regions of the output spike train). This activity is much more faithful to the behaviour observed in the cortex.

The Fano factor was computed numerically once again using a counting window of $T = 100$ms and $w = 1.55$. The value was found to be approximately $F(T) = 1.03$ which is indeed closer to the value found in the cortex (tends to be slightly larger than 1). Since we had again fine-tuned our choice of w to achieve an output firing rate close to 10Hz, the denominator of the expression for the Fano factor (Equation 27) remained the same at around $r_T = 1$. This indicates that the increase in the Fano factor is due to an increase in the variance of the output spiking, which was found to be around $\sigma_T^2 = 1$.

The increase in the spiking variance has been achieved thanks to the decreased mean of the membrane potential, which now coincides with the reset voltage of the spike-and-reset mechanism (i.e. 0). This means that the reset routine does not disrupt the stationary activity of the membrane potential, stopping it from having to return to stationarity through a transient phase as the neurons in Section 3 do. This allows the output spiking to be more variable as we can now have several spikes in each 100ms window. This is in contrast to the model in Section 3 where a neuron has to wait for the transient after a reset to decay before it can fire once again.

5 Full Network

In this final section, we implement the full network as specified in the Introduction. The discrete dynamics of the membrane potential of a particular neuron i in population α are described by

$$\widetilde{V}_i^{\alpha}(k) \leftarrow \widetilde{V}_i^{\alpha}(k-1) + \delta_t \left[-\frac{\widetilde{V}_i^{\alpha}(k-1)}{\tau} + \sum_{\beta \in \{\text{E,I,X}\}} \frac{J_{\alpha\beta}}{\sqrt{K}} \sum_{j \in C_i^{\alpha\beta}} \widetilde{S}_j^{\beta}(k-1) \right] \tag{40}$$

which involves generating random connectivity represented by the set $C_i^{\alpha\beta}$ which randomly selects K indices of presynaptic partners from population β to connect into the i^{th} neuron in population α. Throughout this section we work with the parameter values listed in Table 1 and the following values for the synaptic weight parameters

$$\begin{gathered} J_{EE} = 1,\ J_{EI} = -2,\ J_{EX} = 1, \\ J_{IE} = 1,\ J_{II} = -1.8,\ J_{IX} = 0.8 \end{gathered} \tag{41}$$

5.1 Part A

The theoretical arguments developed in the lecture state that to achieve finite-mean inputs with fixed non-degenerate weights the following equation must be satisfied

$$\begin{cases} J_{EE} r_E + J_{EI} r_I + J_{EX} r_X = \mathcal{O}(1/\sqrt{K}) \to 0 \\ J_{IE} r_E + J_{II} r_I + J_{IX} r_X = \mathcal{O}(1/\sqrt{K}) \to 0 \end{cases} \tag{42}$$

as $K \to \infty$. These equations arise from the fact that the mean of the inputs for a neuron in E or I can be easily seen from Equation 40 to be

$$\begin{cases} \mu_E = \sqrt{K}(J_{EE} r_E + J_{EI} r_I + J_{EX} r_X) \\ \mu_I = \sqrt{K}(J_{IE} r_E + J_{II} r_I + J_{IX} r_X) \end{cases} \tag{43}$$

and this model is known to self-regulate the rates of excitatory and inhibitory activity to ensure that the means of the inputs remain finite for any value of K, if a non-degenerate set of synaptic weight parameters J is selected (van Vreeswijk and Sompolinsky, 1996). This implies that the sum of the products of the weights and their corresponding rates have to be of order $\mathcal{O}(1/\sqrt{K})$ to avoid the means μ_E and μ_I from becoming infinite for large K. This gives us the linear simultaneous equations in Equation 42.

If the rate of the external neurons is $r_X = 10$Hz and if we take the synaptic weight parameters to have the values in Equation 41 (which are known not to be degenerate) we have a simple system of equations governing the firing rates of the excitatory population r_E and the inhibitory population r_I. Assuming large K, these can be easily solved to find their corresponding values when $r_X = 10$

$$\begin{cases} r_E - 2r_I + 10 = 0 \\ r_E - 1.8 r_I + 8 = 0 \end{cases} \tag{44}$$

which gives

$$r_E = r_I = r_X = 10 \tag{45}$$

5.2 Part B

The full network was simulated for 2 seconds for $r_X = 10$Hz using $K = 100$ input neurons from each population and a total number of $N = 1000$ neurons in each of the three populations. The activity of the neurons in populations E and I is plotted from various perspectives in the following plots

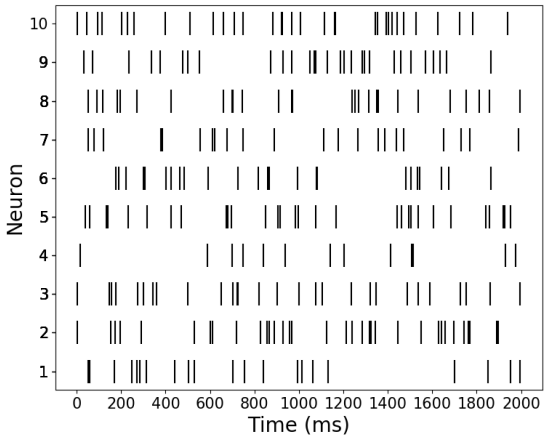

(a) Raster plot over 2 seconds for 10 neurons.

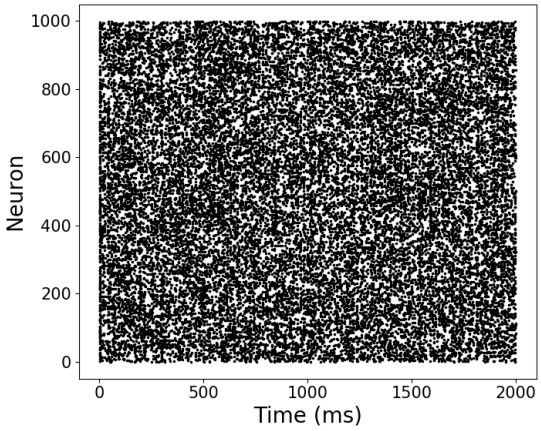

(b) Raster plot over 2 seconds for $N = 1000$ neurons.

Figure 11: Raster plots over 2 seconds for (a) 10 and (b) 1000 excitatory neurons from the full network implementation. From the plots, we can observe an average of approximately 20 spikes over the course of the 2 seconds, as expected.

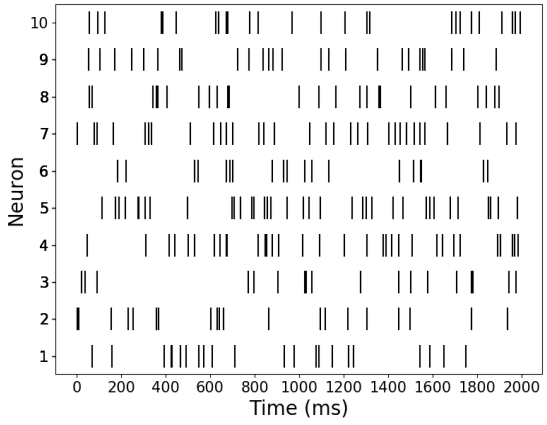

(a) Raster plot over 2 seconds for 10 neurons.

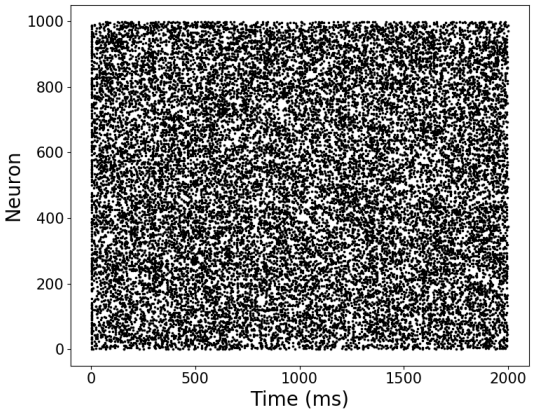

(b) Raster plot over 2 seconds for $N = 1000$ neurons.

Figure 12: Raster plots over 2 seconds for (a) 10 and (b) 1000 inhibitory neurons from the full network implementation. From the plots, we can observe an average of approximately 20 spikes over the course of the 2 seconds, as expected.

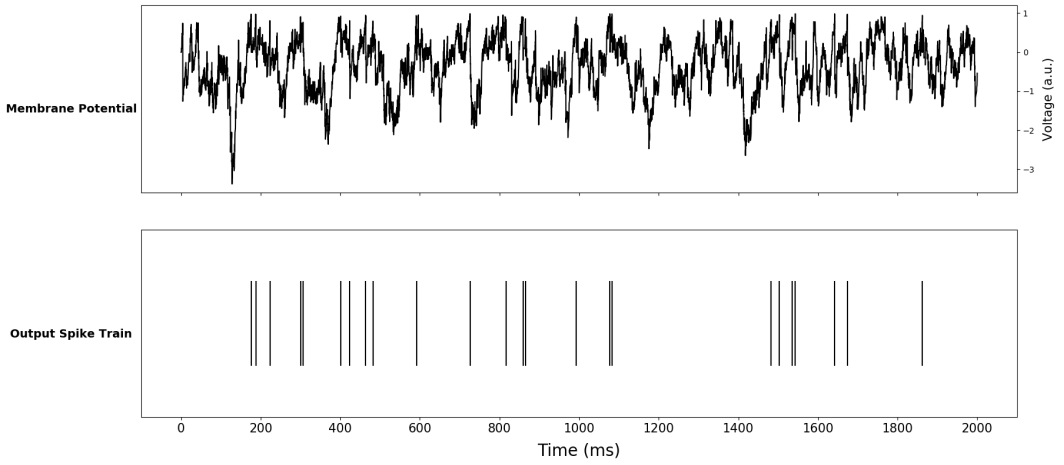

Figure 13: Plot of the membrane potential (top) and output spike train (bottom) of an excitatory LIF neuron receiving inputs from $K = 100$ excitatory, inhibitory and external neurons with the synaptic weights given in Equation 41.

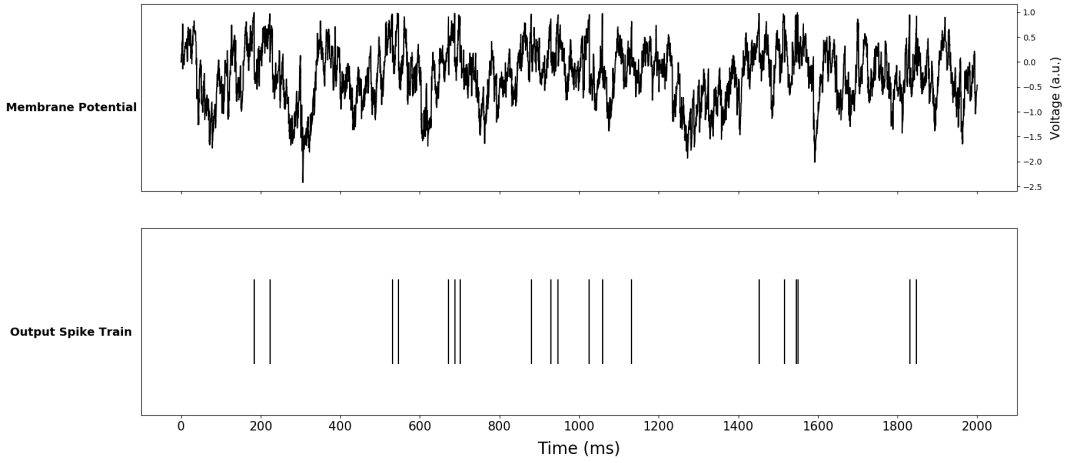

Figure 14: Plot of the membrane potential (top) and output spike train (bottom) of an inhibitory LIF neuron receiving inputs from $K = 100$ excitatory, inhibitory and external neurons with the synaptic weights given in Equation 41.

After implementing the full network, the theoretical values of $r_E = 10$Hz and $r_I = 10$Hz were found to agree quite well with the empirical values calculated from the simulation, which on average gave $r_E = 12.89$Hz and $r_I = 11.58$Hz. The agreement is not perfect but nevertheless similar in terms of order of magnitude. The reason for this discrepancy is the finite value of $K = 100$ which clearly does not cause the right hand side of Equation 42 to be equal to 0. In fact, a correction factor for finite K is proposed in van Vreeswijk and Sompolinsky (1996) based on mean field theory, which allows you to obtain more precise values of r_E and r_I for finite K.

It was interesting to note that the inhibitory rate was consistently lower than the excitatory firing rate over several runs of the simulation. This was also observed in the subsequent sections when the experiment was repeated with different values of r_X. This can be explained by observing the mean of the membrane potential of neurons in the inhibitory population, which is lower than that for the excitatory population and hence causes them to cross the positive spiking threshold of $V_{th} = 1$ less often than the excitatory neurons. This consequently lowers their mean firing rate as compared to the those of excitatory neurons.

5.3 Part C

According to theory, r_E and r_I would depend on r_X as dictated by the system of equations in Equation 42, which yields the following expression linking the rates

$$r_X = r_E = r_I. \tag{46}$$

To assess how closely the empirical values of r_E and r_I agree with r_X, we ran the simulation several times changing the value of r_X in the set $[5, 10, 15, 20]$ after every run. The results of this experiment are tabulated below

Table 3: Table showing the empirical values of r_E and r_I for different values of r_X.

Dependence of r_E and r_I on r_X		
r_X	r_E	r_I
5Hz	7.05Hz	5.85Hz
10Hz	12.89Hz	11.58Hz
15Hz	18.54Hz	17.00Hz
20Hz	24.09Hz	22.39Hz

we also plot this data in Figure 15

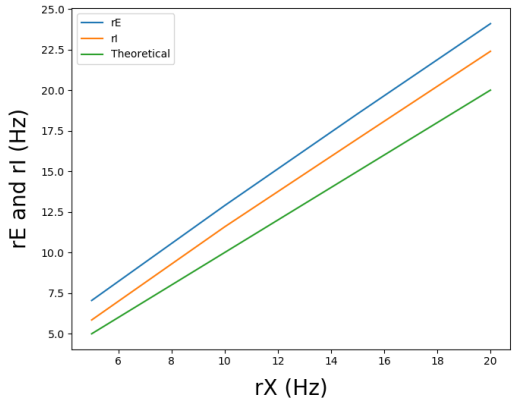

Figure 15: Comparison of theoretical (green) and empirical values for the rates of neurons in the excitatory r_E (blue) and inhibitory r_I (orange) populations as a function of r_X. Note how the empirical values of r_E and r_I are always greater then r_X and that the discrepancy between them grows for increasing r_X.

We note that the values of r_E and r_I are always larger than their theoretical predicted values. Once again, this is due to the finite value of K which causes the right hand side of Equation 42 to be greater than 0 and hence increases the value of r_E and r_I for a fixed r_X. This is shown by assuming that we have small constants a and b on the RHS of Equation 42

$$\begin{cases} r_E - 2r_I + r_X = a \\ r_E - 1.8r_I + 0.8r_X = b \end{cases} \tag{47}$$

where a and b are small deviations from the original assumed value of 0 which give the following solutions

$$r_E = r_X + 10(b - a) \text{ and } r_I = r_X + 5(b - a) \tag{48}$$

This would explain why the rates are always larger than their theoretical prediction of $r_E = r_I = r_X$ if $b > a$, which seems to be the case. This would also explain why the inhibitory is always lower than the excitatory rate. We also note that increasing r_X led to values of r_E and r_I that increasingly diverge from themselves and from their theoretical predictions. This can be explained using the correction for finite K described in van Vreeswijk and Sompolinsky (1996).

5.4 Part D

Upon setting the number of neurons in each population to $N = 100$ and the number of neurons chosen to connect into each neuron to be $K = 100$, we observe complete synchronicity among all the neurons in the same population. This can be seen in the population dynamics presented below

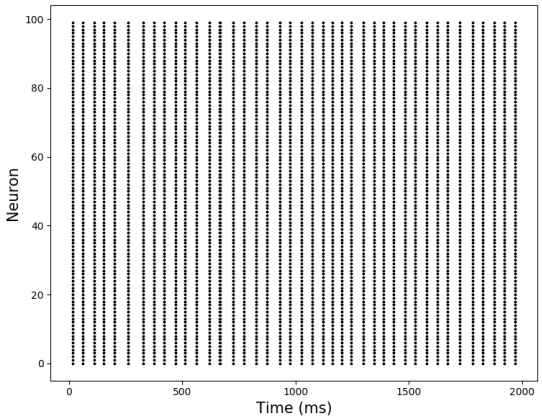

(a) Raster plot for $N = 100$ excitatory neurons.

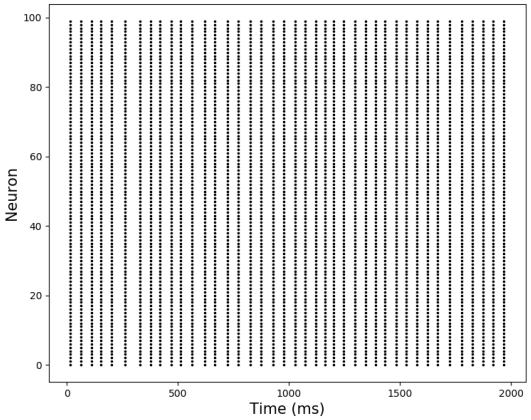

(b) Raster plot for $N = 100$ inhibitory neurons.

Figure 16: Raster plots over 2 seconds for 100 (a) excitatory and (b) inhibitory neurons from the full network implementation with $N = K = 100$. From the plots, we can observe complete population synchronicity.

and for a single neuron we observe a regular firing pattern and a repeated pattern in the voltage fluctuations

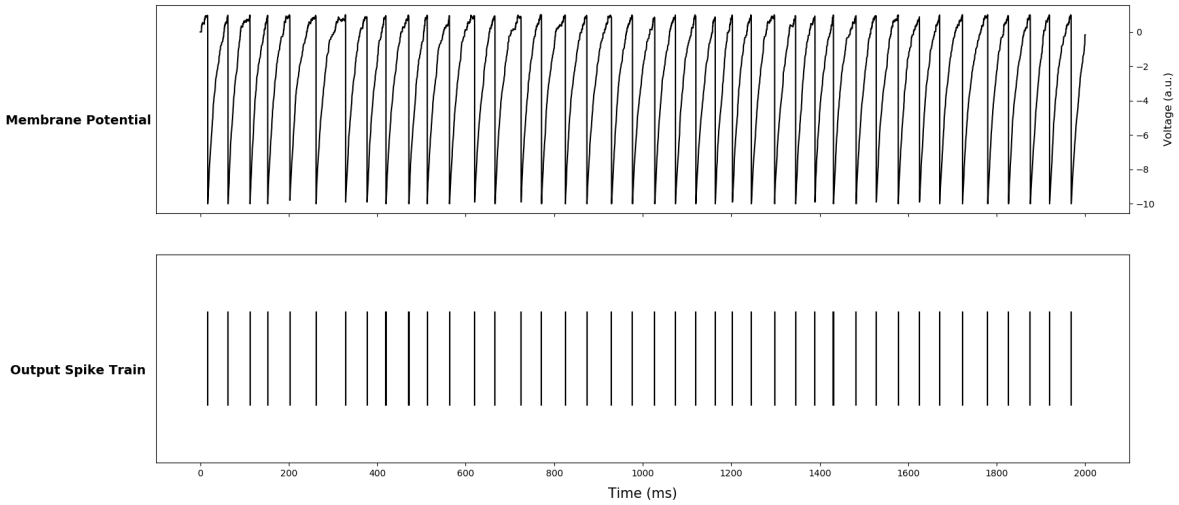

Figure 17: Membrane potential (top) and output spike train (bottom) for 2s of a single excitatory neuron when $N = K = 100$. Note how every time we observe a spike, we actually observe a spike "couple" (i.e. two spikes occurring in subsequent timesteps) and this occurs at regular time intervals across the entire duration of the simulation. Note that this was not observed in the inhibitory neurons. We also observe a regular pattern in the membrane potential which (i) reaches the spiking threshold, (ii) decreases sharply to -10 and then (iii) increases towards the threshold again.

This phenomenon arises because the network is fully connected when we set $K = N$, meaning that every neuron in E and I connects to every other neuron in each of the three populations E, I and X. They hence all receive the same inputs, which causes them to have the same dynamics. Analysing the behaviour of the implementation in more detail reveals that the code is sequencing through the following steps:

1. The spike trains of the $N = 100$ Poisson neurons from the X population are sampled independently from rate $r_X = 10$ Poisson processes for the entire duration of the simulation.
2. The voltages and spike trains of the excitatory and inhibitory neurons are initialised to all 0-vectors. Note in particular that they are all equal.
3. In all subsequent iterations of the update equations all E neurons and I neurons will continue to have the same membrane potential values as they all have the same inputs (i.e. all the neurons from each population).
4. If a neuron in X fires, the input to excitatory neurons is $\frac{1}{\sqrt{K}} J_{EX} = 0.1$ and the input to inhibitory neurons is 0.08. This means that in general the E neurons will always fire before the I neurons fire.
5. If an E neuron fires, all E neurons will fire at the same time since they have identical membrane potentials, so in the next timestep the input to the E neurons will be approximately $\frac{1}{\sqrt{K}} J_{EE} K = 10$, and the input to I neurons from the E population will be 8.
6. This means that in the next timestep both the E and I population will fire again. However, the input to E neurons in the subsequent timestep will be $\frac{1}{\sqrt{K}}(J_{EE} + J_{EI})K = -10$ and the input to I neurons will be -8.
7. Hence from the next timestep the membrane potentials of both E and I neurons slowly return to 0.

This is what causes the regular firing of "spike couples" (i.e. spikes that fire only one timestep away from each other) in excitatory neurons that can be seen in Figure 17. This also explains why the excitatory neurons have a firing rate that is twice that of inhibitory neurons at $r_E = 40$Hz and $r_I = 20$Hz. We have violated the condition that an important aspect of the architecture is the random, sparse connectivity of the network. Although the average number of projections, K, can be large, it must still be smaller than the total number neurons in each population N.

Conclusion

In this report we have discussed the benefits, disadvantages and caveats of the three population model proposed by van Vreeswijk and Sompolinsky (1996). We have seen that, in its full implementation, it balances the rates of excitatory and inhibitory spike trains to give finite input means and hence promote stability in the network. We have also seen that it produces a Fano factor which is comparable to that encountered in the real cortex. Both of these are important properties that are observed in brain network dynamics and which this model can successfully recreate under mild assumptions.

References

L. Lapicque. Recherches quantitatives sur l'excitation electrique des nerfs traitée comme une polarization. *Physiol Pathol Gen (Paris)*, (9):620–635, 1907.

C. van Vreeswijk and H. Sompolinsky. Chaos in neuronal networks with balanced excitatory and inhibitory activity. *Science*, 274(5293):1724–1726, 1996. ISSN 0036-8075. doi: 10.1126/science.274.5293.1724. URL `https://science.sciencemag.org/content/274/5293/1724`.